Alkaline treatment combined with enzymatic hydrolysis for efficient cellulose nanofibrils production

Gabriel Banvillet, Gaël Depres, Naceur Belgacem, Julien Bras

Alkaline treatment combined with enzymatic hydrolysis for efficient cellulose nanofibrils production

Gabriel Banvillet[1,2], Gaël Depres[2], Naceur Belgacem[1,3], Julien Bras[1,3,4]

1 Univ. Grenoble Alpes, CNRS, Grenoble INP*, LGP2, F-38000 Grenoble, France

2 Arjowiggins France SAS, Voiron F-38500, France

3 Institut Universitaire de France (IUF), Paris F-75000, France

4 Nestle Research Center, Lausanne 1100, Suisse

* Institute of Engineering Univ. Grenoble Alpes

Abstract

Cellulose nanofibrils were efficiently produced from eucalyptus fibers using a combined NaOH and enzymatic treatment followed by a pilot scale grinding process. The structural changes of fibers were assessed after NaOH treatments at 5, 10 and 15 wt% concentrations. A progressive shift from a cellulose I to a cellulose II crystalline structure was observed with X-ray diffraction (XRD) and nuclear magnetic resonance (NMR). The further enzymatic hydrolysis was improved for the NaOH treated samples. The increase of crystallinity indices due to enzymatic hydrolysis was of + 4.7 %, + 3.5 %, and +10.3 % for samples treated with NaOH 5, 10 and 15 wt% respectively, and DP values were drastically reduced to 340, 190 and 166 respectively. A morphological analysis underlined an optimum with the combination of NaOH 10 wt% and enzymatic hydrolysis. This treatment followed by the grinding process resulted in CNF with a rigid structure, with diameters ranging from 10 to 20 nm and lengths between 150 and 350 nm. A multi-scale analysis enabled to study the impact of this combined treatment on CNF properties and energy consumption. A decrease in mechanical properties of nanopapers was observed for the combined treatment and NaOH treatment alone compared to enzymatic hydrolysis alone, with Young's modulus of 8.94, 4.84 and 11.21 GPa respectively. However, optical properties were improved, with transmittance values of 42.2, 15.4 and 7.1 % respectively. This new pretreatment can therefore lead to CNF with tunable properties depending on the application, with possible industrialization thanks to the reduction of energy needs.

Keywords

Cellulose nanofibrils, sodium hydroxide, enzymatic hydrolysis, fiber morphology, nanopapers.

Highlights

- alkaline treatments facilitated the further enzymatic hydrolysis of cellulose fibers.
- combined NaOH and enzymatic treatments easily led to a CNF network after grinding.
- mechanical properties of CNF were negatively affected by the combined treatments.
- optical properties of CNF were positively affected by the combined treatments.

1. Introduction

Cellulose is produced in nature by a wide variety of organisms, and is the main structural element in the cell wall of majority of plants. It composes a large portion of wood, cotton, hemp, linen, ramie, etc. This biopolymer is thus produced in considerable quantities each year, with an estimated annual production by terrestrial plants of 50.10^9 tons. The total available cellulose is estimated to be more than 10^{11} tons (Stevanovic, 2016), making it the most abundant polymer on Earth. Natural cellulose fibers, which are relevant for applications such as paper or textile, can be processed into nanoscale elements by the use of chemical, enzymatic and/or mechanical treatments (Nechyporchuk et al., 2016). The obtained nanocellulose, with rigid highly crystalline (cellulose nanocrystals, CNC) or flexible semi-crystalline structure (cellulose nanofibrils, CNF) exhibit interesting mechanical, optical, rheological and barrier properties. CNF, in particular, have been discovered in the 1980's (Turbak et al., 1983) and considered relevant for a wide range of applications, such as composite reinforcement (Miao & Hamad, 2013), food packaging (Azeredo et al., 2017) or barrier and active coatings (Ferrer et al., 2017; Spieser et al., 2020). They appear as a potential alternative to oil-based products, and could be a major actor of the bioeconomy, as attested by the several national and international development projects from the last decade.

The industrial production of CNF, however, still needs to overcome some issues. Despite the recent improvements concerning chemical pretreatments (Inamochi et al., 2017; Rol et al., 2018), enzymatic hydrolysis (Hu et al., 2018) or mechanical fibrillation (Rol et al., 2020a; Taheri & Samyn, 2016; Tsalagkas et al., 2018), the production volumes remain low, and the CNF price cannot compete with synthetic polymers (Assis et al., 2018). These issues can be explained on one hand by the limitations in CNF quality observed with pretreatments which are easy to be upscaled, such as enzymatic hydrolysis. The discovery of this pretreatment was a major breakthrough for CNF production (Henriksson et al., 2007; Pääkkö et al., 2007), but a plateau in CNF properties is often obtained by this mean (Nechyporchuk et al., 2015; Siqueira et al., 2010). On the other hand, the highly interesting properties obtained by chemical grafting such as TEMPO-oxidation (Saito & Isogai, 2006), carboxymethylation (Kaldéus et al., 2018) or phosphorylation (Rol et al., 2020b) are usually

associated with time-consuming processes, using in some cases toxic chemicals. There is therefore a need to develop and improve new pretreatments in terms of CNF properties and process ease, by using recyclable solvents and up scalable processes.

To this end, the use of aqueous sodium hydroxide (NaOH) as a pretreatment for CNF production has been proposed since the early 2010s. The use of alkaline solutions on native cellulosic fibers is not new, and was first reported more than one century ago in 1850 by John Mercer, who observed an improvement of the properties of cotton fibers treated with a NaOH solution. This patented treatment (Mercer, 1850), named mercerisation after its inventor, was proven to enhance fibers lustre, smoothness, dimensional stability and mechanical properties. Since then, the use of NaOH has expanded to the textile industry, the production of regenerated cellulose, or even the cellulose dissolution. Its action on cellulose is nowadays well documented, and consists in a conversion from the native cellulose I structure to the thermodynamically more stable cellulose II structure. This phenomenon takes place with a swelling of cellulose fibers by NaOH hydrates and the formation of alkali complexes. This results in a shift from a parallel crystalline conformation (cellulose I) to an antiparallel one (cellulose II) through translation diffusion mechanisms, although the physical state of cellulose during this reaction is still not fully understood (Budtova & Navard, 2016). The conversion to cellulose II is irreversible, and the study of its crystalline structure by X-ray and neutron diffraction highlighted a greater number of hydrogen bonds in this conformation (Pérez & Mazeau, 2005).

Alkaline treatment on previously individualized CNF was reported in 2011 (Abe & Yano, 2011) resulting in high-strength hydrogels compared to untreated cellulose. Dissolution of CNF in aqueous NaOH was also performed in 2015 (Yamane et al., 2015), leading to a stable cellulose solution in terms of viscosity. However, the use of NaOH treatment alone for CNF production was first reported by Wang et al., 2014. The process was composed of a mercerisation step in 17.5 wt% NaOH for 12 hours, followed by several passes in a grinder and a homogenizer. The obtained CNF, with 15 - 100 nm widths, had better thermal stability compared to untreated fibers, but lower mechanical properties (Young's modulus of 8.6 and 11.8 GPa respectively). Later, this treatment was adapted with simultaneous ball-milling (Abe, 2016, 2019) leading to stable hydrogels but poorly individualized CNF due to quick gelation. Under the form of films, the CNF exhibited lower mechanical properties compared to typical CNF films, but the continuous network formed and possibility to tune the properties with controlled crystalline structures were underlined. These studies were of great interest as they showed the possibility to obtain CNF with a simple NaOH treatment. The remaining issues were (i) the difficulty to individualize CNF due to the gelation during NaOH treatment and (ii) the medium quality of the resulting CNF.

The use of enzymatic hydrolysis of cellulose along with alkaline treatment has been explored recently. An enzymatic hydrolysis prior to dissolution in NaOH was proven to improve the dissolution kinetics and efficiency, due to DP decrease and deconstruction of fibers (Budtova & Navard, 2016; Le Moigne et al., 2010). Inversely, NaOH treatment prior to enzymatic hydrolysis was shown to have a positive effect. The shift to cellulose II was proven to increase cellulose accessibility for enzymes (Kobayashi et al., 2012; Ling et al., 2017), thus improving hydrolysis kinetics (Wada et al., 2010) and yield (Kuo & Lee, 2009; SriBala et al., 2016). An alkaline pretreatment prior to enzymatic hydrolysis was also proven to be efficient for CNF production from soybean straw (Martelli-Tosi et al., 2016). In this study, the alkaline pretreatment is coupled with a bleaching step using sodium chlorite or hydrogen peroxide. A laboratory scale mechanical treatment (Ultra Turrax) enabled the production of CNF with 8-12 nm widths as observed with transmission electron microscopy. However, according to the authors, the combination of alkaline and enzymatic treatments has not been clearly applied to a pilot scale CNF production process.

This study aims to investigate the relevance of a combined NaOH and enzymatic treatments for CNF production. To that end, three NaOH treatments at 5, 10 and 15 wt% were performed on refined kraft bleached eucalyptus fibers, followed by enzymatic hydrolysis with an endoglucanase. The term mercerisation was not used, as it refers to NaOH treatments under specific conditions (NaOH 18 - 32 wt%, temperature 25 - 40 °C, short treatment time) that were not used here. The crystalline structure of cellulose was studied by X-ray diffraction and nuclear magnetic resonance, to assess the shift from cellulose I to cellulose II, and to quantify the improvement of enzymatic hydrolysis. Fiber morphology was investigated with scanning electron microscopy, MorFi analysis and degree of polymerization. Optimal pretreatment conditions were determined and the pretreatment was adapted to a pilot reactor. Cellulose nanofibrils were thereafter produced with a grinding treatment, and CNF properties were studied as suspensions and films, to assess the combined pretreatment efficiency compared to NaOH and enzymes alone.

2. Experimental section

2.1 Materials

Bleached Eucalyptus Kraft Pulp was purchased as dry pulp sheets from Cenibra, Brazil. Enzyme solution FiberCare© R (Novozyme, Denmark) with an endoglucanase activity of 4770 ECU/g was kindly supplied by the partner company Arjowiggins, France. Chemicals were used as received from suppliers: sodium hydroxide (NaOH 50 % in H_2O, Sigma-Aldrich), acetic acid (CH_3COOH ≥ 99.7 %, Sigma-Aldrich), sodium acetate trihydrate ($CH_3COONa \cdot 3H_2O$ ≥ 99.0 %, Sigma-Aldrich), hydrochloric

acid (HCl 37 %, Sigma-Aldrich), bis(ethylenediamine)copper(II) hydroxide solution ($Cu(H_2NCH_2CH_2NH_2)_2(OH)_2$ 1.0 M in H_2O, Sigma-Aldrich), sulfuric acid (H_2SO_4 95.0 – 98.0 %, Sigma-Aldrich), potassium iodide (KI ≥ 99.0 %, Sigma-Aldrich), potassium permanganate ($KMnO_4$ ≥ 99.0 %, Sigma-Aldrich), sodium thiosulfate ($Na_2S_2O_3$ 99 %, Sigma-Aldrich).

2.2 Cellulose alkaline and enzymatic treatment

2.2.1 Pulping and refining

Cellulose fibers were dispersed with deionized water into a 2 wt% suspension with a laboratory scale pulper for 10 minutes. Refining was performed with a Valley beater (Voith, Germany) until a fibrillation degree of 70 SR as measured with a Shopper Riegler tester (Paper Testing Association, France) following the ISO 5267-1 standard. The pulp was then filtered with a nylon sieve with a mesh size of 1 µm until a concentration of 10 wt%.

2.2.2 NaOH treatment

Refined cellulose fibers were treated with three different sodium hydroxide solutions, with NaOH concentrations of 5, 10 and 15 wt% respectively. The reactions were performed under stirring at room temperature for 1 h, with a pulp solid content of 2 wt% (20 g pulp, 980 g NaOH solution). The NaOH solutions with various concentrations were prepared by diluting a NaOH 50 wt% solution with deionized water, considering the water present in the pulp. After the reaction, the suspensions were filtered once with a Buchner funnel using a nylon sieve with a mesh size of 1 µm, and dispersed at 2 wt% with deionized water. The residual sodium hydroxide was neutralized with a 0.5 M HCl solution. Filtration and neutralization steps were repeated several times until a stable pH of 7.0 was obtained. The 10 wt% NaOH treatment was adapted to 200 g of fibers, with the same protocol adapted to a 12 L reactor. 100 g were recovered for direct fibrillation into the grinder, and 100 g were further treated with enzymes before fibrillation into the grinder.

2.2.3 Enzymatic hydrolysis

Enzymatic hydrolysis was performed on refined pulp as such, and after NaOH treatments at concentrations of 5, 10 and 15 wt% respectively. 10 g of pulp were introduced with a solid content of 2 wt% in a reaction flask under mechanical agitation. A temperature of 50 °C was set with an oil bath, and a stable pH of 5.0 was obtained with an acetate buffer composed of acetic acid and sodium acetate trihydrate. The enzyme solution (FiberCare R cellulase with an activity of 4770 ECU/g of solution) was then poured into the reaction flask, with an enzyme concentration of 300 ECU/g of cellulose (6.29×10^{-2} g of enzyme solution / g of cellulose). After 2 hours of reaction, the enzymatic hydrolysis was stopped by diluting the pulp suspension to 1 wt% with boiling deionized water during

5 minutes. The pulp was filtered with a Buchner funnel using a nylon sieve with a mesh size of 1 µm. Additional washing and filtration steps were performed, in order to remove the residual salts and the sugars produced during the reaction. The pulp with a solid content of approximatively 20 wt% was then carefully recovered from the nylon sieve and stored in fridge. The enzymatic hydrolysis on NaOH 10 wt% treated pulp was adapted to 100 g of fibers, with the same protocol adapted to a 12 L reactor, before fibrillation into the grinder.

2.2.4 Process yields

The process yields were calculated for each reaction with the following equation:

$$\text{yield}\ (\%) = \frac{m_f}{m_i} \times 100 \qquad (1)$$

where m_i is the initial dry mass of fibers in grams and m_f the final dry mass of (nano)fibers in grams. For processes including several steps, *e.g.* coupled NaOH treatment and enzymatic hydrolysis, the initial mass corresponds to the dry mass of refined fibers before any reaction, and the final mass corresponds to the dry mass of fibers after both process steps.

2.3 CNF preparation

2.3.1 Mechanical fibrillation processes

Two fibrillation processes were used for the deconstruction of fiber structure: (i) a mild and low shear laboratory scale mechanical fibrillation process (Ultra Turrax T-25 disperser, IKA, Germany) to assess the pretreatments efficiency on a small quantity of fibers, and (ii) a pilot scale ultra-fine friction grinder (Model MKZA6-2, Disk model MKG-C 80, Masuko Sangyo Co., Ltd., Japan) for an efficient high-quality CNF production. The Ultra Turrax mechanical treatment was performed on 5 g of pulp with a solid content of 2 wt%, with a rotation speed of 8,000 rpm and 10 min treatment time at room temperature. Samples before and after the mechanical treatment were recovered, in order to study its impact on fiber morphology and creation of CNF. The ultra-fine friction grinding treatment was performed on 100 g of pulp with a solid content of 2 wt%, with a rotation speed of 1,500 rpm. The pressure between rotor and stator disks was determined with the apparatus arbitrary units. A progressive shift from graduation 0 (low pressure) to graduation 20 (high pressure) was achieved, for a total number of passes between 30 and 40. For the sample treated with both NaOH 10 wt% and enzymes, the graduation 30 could be used without process issues. The specific energy consumption was calculated with the Equation 2:

$$\text{Specific Energy Consumption}\ (\text{MWh/t}) = \frac{P_{net} \times t}{m_{dry}} \qquad (2)$$

where P_{net} is the net power (MW) measured during the mechanical treatment, t the fibrillation time (h) and m_{dry} the dry mass of fibers (t). The net power and fibrillation time were measured for each graduation used, and the specific energy consumptions were summed to obtain the total energy consumption of the process. The energy consumption of the refining step (approx. 0.6 MWh/t) was considered. Samples were recovered at different stages of the process for further characterization.

2.3.2 Preparation of nanopapers

Nanopapers (60 g/m²) were prepared by filtration using a Rapid Köthen sheet former. 2 g of CNF were diluted to 0.5 wt% with deionized water and homogenized for 1 min with an Ultra Turrax T-25 disperser at 8,000 rpm. The suspension was then filtered with the sheet former equipped with an additional nylon sieve with a mesh size of 1 µm, under a controlled vacuum of – 500 mbar. After a complete removal of water, the CNF sheets were dried between two nylon sieves under vacuum at 85 °C for 20 min. 2 nanopapers were made for each CNF suspension. The nanopapers were stored in a conditioned room at 23 °C and 50 %RH for 48 h before any characterization.

2.4 Cellulose fibers and nanofibrils characterization

2.4.1 MorFi analysis

Fiber morphology was analyzed with a MorFi LB-01 fiber analyzer (Techpap, France). 300 mg of pulp were diluted in 7 L of water and kept under constant recirculation in the image acquisition system. The fiber / fine limit was set to 200 µm in length, and the analysis was carried out until 5,000 fibers were detected. The analysis was done twice on each sample, and average fiber length (µm) and fine content (% in area) were determined.

2.4.2 Optical microscopy

Optical microscopy images were acquired with a microscope Axio Imager M1 (Carl Zeiss, Germany) equipped with an AxioCam MRc 5 digital camera. Before slide preparation, suspensions were diluted to 0.1 wt%. Magnifications of x50 and x100 were used, at least 8 images were taken for each magnification and the most representative were selected.

2.4.3 Scanning Electron Microscopy (SEM)

Fiber and CNF suspensions were diluted to 0.1 wt%, dried under vacuum on a carbon adhesive and coated with a 5 nm Au/Pd layer. For the study of fiber morphology, images were acquired with an ESEM Quanta 200 (FEI, Japan) in ETD mode. A working distance of 10 mm and an acceleration voltage of 10.0 kV were used. At least 15 images by sample were acquired, with magnifications between × 100 and × 4,000, and the most representative ones were selected. For the study of CNF morphology,

images were acquired with a FEI Quanta 250 equipped with a field emission gun in ETD mode. A working distance of 8 mm and an acceleration voltage of 2.50 kV were used. At least 10 images by sample were acquired, with magnifications between × 5,000 and × 40,000, and the most representative ones were selected.

2.4.4. Transmission Electron Microscopy (TEM)

Transmission electron microscopy images were acquired on the supernatant of CNF suspensions at 0.1 wt% after 24 hours of settling, to avoid the presence of micrometric fragments during sample preparation. Droplets of dilute CNF suspension were deposited onto glow-discharged carbon-coated TEM grids. After a few minutes, the liquid in excess was blotted with filter paper and, prior to drying, the preparation was negatively stained with 2 wt% uranyl acetate. The stain in excess was blotted and the specimen allowed to dry. Images were recorded with a JEOL JEM-2100-Plus microscope operating at 200 kV equipped with a Gatan Rio 16 digital camera. Images were further analyzed with the software Fiji – ImageJ for the determination of CNF length and diameter, at least 50 measurements were performed.

2.4.5 Chemical composition

The lignin content was determined with the micro-kappa number following the TAPPI T 236 om-13 standard. 2 g of sample were diluted in 150 mL of deionized water, and 20 mL of sulfuric acid 4 N were added. 20 mL of potassium permanganate 0.05 N were added and the suspension was allowed to react for 10 min at a temperature of 25 °C, controlled with a water bath. 10 mL of potassium iodide 1 M were then added to stop the reaction, and the remaining permanganate was titrated with sodium thiosulfate 0.05 N. The micro-kappa number was calculated using the following formula:

$$\text{Micro-kappa} = \left[\frac{(V_1 - V_2) \times 0.05}{0.1}\right] \times \frac{D}{m} \qquad (3)$$

where V_1 is the added volume of sodium thiosulfate for the blank test without pulp, V_2 is the added volume of sodium thiosulfate for the test with pulp, m is the dry mass of pulp, and D a correction coefficient. The lignin content was calculated with the formula:

$$\text{Lignin content}\ (\%) = 0.147 \times \text{micro-kappa} \qquad (4)$$

The cellulose and hemicellulose contents were adapted from the TAPPI T 203 cm-99 standard. 2 g of oven dried pulp were dispersed in 100.0 mL of NaOH 17.5 % in a 500 mL flask, at a temperature of 25 °C controlled with a water bath. After 30 min of reaction, 100.0 mL of deionized water were added and the suspension was allowed to react for another 30 min. The pulp was then recovered and

washed several times with deionized water in a Buchner funnel using a 1 µm nylon sieve. The α-cellulose content was calculated with the following formula:

$$\alpha\text{-cellulose content}\ (\%) = \frac{m_1}{m_0} \times 100 \qquad (5)$$

where m_0 is the initial mass of pulp and m_1 the mass of pulp after treatment. The estimated hemicellulose content was then calculated by subtraction, knowing the α-cellulose and lignin contents in the pulp. The analyses were duplicated and the average values were calculated.

2.4.6 Degree of polymerization

Degree of polymerization (DP) was determined following the ISO 5351:2010 standard. Fibers were dissolved in a bis(ethylenediamine)copper(II) hydroxide solution, and intrinsic viscosity [η] in mL/g was measured with a capillary viscometer. The viscosity average DP_v was calculated using the Mark-Houwink-Sakurada equation:

$$DP_v^{0.905} = 0.75 \times [\eta] \qquad (6)$$

An average DP value was calculated from triplicates.

2.4.7 X-ray diffraction

Prior to X-ray diffraction and nuclear magnetic resonance, fibrous samples were milled into powder form by cryocrushing. 1 g of sample was cryocrushed for 2 minutes with 2 zirconium balls in a 20 mL chamber cooled with liquid nitrogen, with an oscillation frequency of 30 Hz. An amorphous reference was produced by cryocrushing raw fibers during 20 min under similar conditions. Powders were deposited on a zero-background Si substrate, and X-ray diffraction (XRD) was performed using a diffractometer X'Pert Pro MPD (PANalytical, Netherlands) equipped with a Bragg-Brentano geometry. A copper anode (Kα λ = 1.5419 Å) was used, with the angle 2θ ranging from 6° to 60° with a 0.05° interval. The crystallinity index was calculated by amorphous subtraction with the following formula:

$$CI\ (\%) = \frac{A_c}{A_c + A_a} \times 100 \qquad (7)$$

where A_c corresponds to the crystalline area of the XRD pattern, and A_a to the amorphous area of the XRD pattern (amorphous reference). The crystalline area is therefore obtained by subtracting the area of the amorphous reference to the area of the sample's total XRD pattern.

2.4.8 Nuclear magnetic resonance

Solid-state ^{13}C Nuclear Magnetic Resonance (^{13}C NMR) was performed on a spectrometer Avance 500 (Bruker, USA) using cross-polarization, high power proton decoupling and magic angle spinning (CP-

MAS). Spectra were acquired at 25 °C, with a 4 mm probe operating at 125.78 MHz for ^{13}C and 500.18 MHz for ^{1}H. Samples were placed in a 4 mm ZrO_2 rotor, and the acquisition was made with a number of scans of 40,000, relaxation time of 2.0 seconds, CP time of 2.0 ms, 12 kHz MAS and 300 ppm spectral width. The crystallinity index was calculated using equation (7) with A_c being the area of crystalline contribution of carbon C_4 (93.0 - 86.2 ppm), and A_a being the area of disordered contribution of carbon C_4 (86.2 – 80.0 ppm).

2.4.9 Turbidity

Suspensions were diluted to 0.1 wt% with deionized water and homogenized for 1 min with an Ultra Turrax T-25 disperser at 8,000 rpm. Turbidity values in Nephelometric Turbidity Units (NTU) were measured with a turbidity meter AL-250 (Aqualytic, Germany). The test measures the scattered light at 90° from an incident light (λ = 860 nm), which is related to the size and shape of the cellulosic fibrous elements of the suspension. At least 9 measurements were done for each sample and the average value was calculated.

2.4.10 Transmittance

The transmittance of CNF nanopapers (in % of the incident light) was measured at a wavelength of 550 nm with a UV-spectrophotometer (Shimadzu Manufacturing, USA) in photometric mode. 5 measurements were done on each nanopaper, 2 nanopapers were analyzed for each sample leading to 10 measurements in total, and the average value was calculated.

2.4.11 Tear resistance

Tear resistance of nanopapers was measured with a tear tester equipped with a 4000 mN pendulum (Noviprofibre, France) in a conditioned room (23 °C and 50 %RH). Samples of 50 × 65 mm² were pre-cut, and the force (in mN) to complete the propagation of the cut was measured. 3 measurements were done on each nanopaper, 2 nanopapers were analyzed for each sample leading to 6 measurements in total, and the average value was calculated.

2.4.12 Tensile test

Tensile properties of nanopapers were measured in a conditioned room (23 °C and 50 %RH) with a dual column testing system 5965 of 50 kN maximum force (Instron, USA), following the NF Q03-004 standard. Samples with dimensions 15 × 100 mm² were tested with a tensile speed of 10 mm/min. The Young's modulus of each sample was calculated using the thickness values of the nanopaper as measured for porosity. 3 measurements were done on each nanopaper, 2 nanopapers were analyzed for each sample leading to 6 measurements in total, and the average value was calculated.

2.4.13 Porosity

The basis weight of each nanopaper was calculated from its mass after 48 h in a conditioned room. Thickness was measured with a Lhomargy micrometer at 8 different positions on the nanopaper, and an average value was calculated. The porosity of the nanopaper was then calculated using the following formula:

$$\text{Porosity}\ (\%) = 1 - \frac{\text{BW}}{\text{e} \times \rho_c} \times 100 \qquad (8)$$

where BW is the basis weight (kg/m²), e the thickness (m) and ρ_c the density of cellulose (1540 kg/m³).

2.4.14 Quality index

As a tool to compare CNF suspensions together, an equation regrouping 5 test values was used, adapted from the publication of Desmaisons et al., 2017. The obtained value named quality index is representative of the global quality of CNF suspensions in terms of optical and mechanical properties. The adapted equation used for quality index calculation was:

$$\text{QI} = 2 \times \text{turbidity mark} + 1 \times \text{transmittance mark} + 2 \times \text{tear resistance mark} + 2 \times \text{Young's modulus mark} + 2 \times \text{porosity mark} + 1 \qquad (9)$$

where marks are calculated from raw test values as indicated in the original publication. The resulting equation including the raw test values was therefore:

$$\text{QI} = -0.02 \times x_1 + 1.65 \times \ln(x_2) - 7.18 \times \ln(x_3) - 0.07 \times {x_4}^2 + 2.54 \times x_4 - 0.32 \times x_5 + 89.96 \qquad (10)$$

where x_1 is the turbidity (NTU), x_2 is the transmittance (%), x_3 is the tear resistance (mN), x_4 is the Young's modulus (GPa), and x_5 is the porosity (%). Nanosized fraction and optical microscopy values were not used for the quality index calculation as compared with the original publication, due to the high standard deviations, poor repeatability of the tests and inaccurate values due to the presence of salts during centrifugation. Higher factors are associated with mechanical properties, leading to a possible difference of ± 3 in the quality index values compared to the values obtained with the original calculation. However, the two values remain very close and comparable, with a reduced standard deviation.

3. Results and discussion

3.1 Influence of NaOH and enzymatic treatments on cellulose crystalline structure

The crystalline structure of cellulosic fibers was first assessed with X-ray diffraction (XRD), before and after NaOH treatments at various concentrations (Fig. 1). The diffraction pattern of 70 SR refined fibers is typical of cellulose Iβ crystalline structure with diffraction peaks at 2θ angles of 15.2°, 16.7°, 22.6° and 34,7°, corresponding to the $(1\bar{1}0)$, (110), (200) and (004) lattice planes respectively (French, 2014; Park et al., 2010). The treatment of cellulose fibers with aqueous NaOH lead to a shift from cellulose I to cellulose II crystalline structures, which is a well-documented phenomenon in the literature (Abe, 2016; Budtova & Navard, 2016; Lee et al., 2018; SriBala et al., 2016; Wang et al., 2014). Diffraction peaks can be observed at 2θ angles of 12.3°, 20.2° and 21.9°, corresponding to the $(1\bar{1}0)$, (110) and (020) lattice planes of cellulose II respectively (French, 2014; Gong et al., 2017; Sèbe et al., 2012). As expected, the intensities of cellulose II peaks increase when NaOH concentration increases, indicating a higher cellulose II content. The sample treated with NaOH 5 wt% exhibits a cellulose I structure with a shoulder at 2θ = 20.2°. The shift from cellulose I to cellulose II is therefore limited for this sample, which is standard in this range of concentration and temperature (Abe & Yano, 2011; Liu & Hu, 2008). The sample treated with NaOH 15 wt%, however, has undergone an almost complete shift to cellulose II. The NaOH 10 wt% treatment results in the presence of both cellulose I and II structures in the sample, with a predominance of cellulose I (Abe & Yano, 2012).

Crystallinity indices (CI) were calculated with an amorphous reference with an area-based method, as the peak height method tends to lead to overestimated values and is not suitable for cellulose II (Ahvenainen et al., 2016; Park et al., 2010). However, it is worth noting that the impact of cryocrushing step on molecular structure before analysis is not negligible. The CI obtained here from the powder form are therefore used only comparatively, and are significantly underestimated compared to the literature. It also should be noted that the CI is representative of the total crystallinity of the sample, irrespective of its cellulose I and cellulose II content.

As described in Table 1, refined fibers have a CI of 40.7 % prior to any treatment. The following NaOH treatments lead to a decrease of CI to 30.2 %, 22.4 % and 18.0 % for 5, 10 and 15 wt% respectively. The impact on crystallinity is more important when NaOH concentration increases, which is due to disruption of the cellulose structure by NaOH hydrates during its conversion into cellulose II form (Lee et al., 2018; Liu & Hu, 2008). The formation of the cellulose II crystalline structure is only partial, and fibers are left in a swollen, globally less organized state.

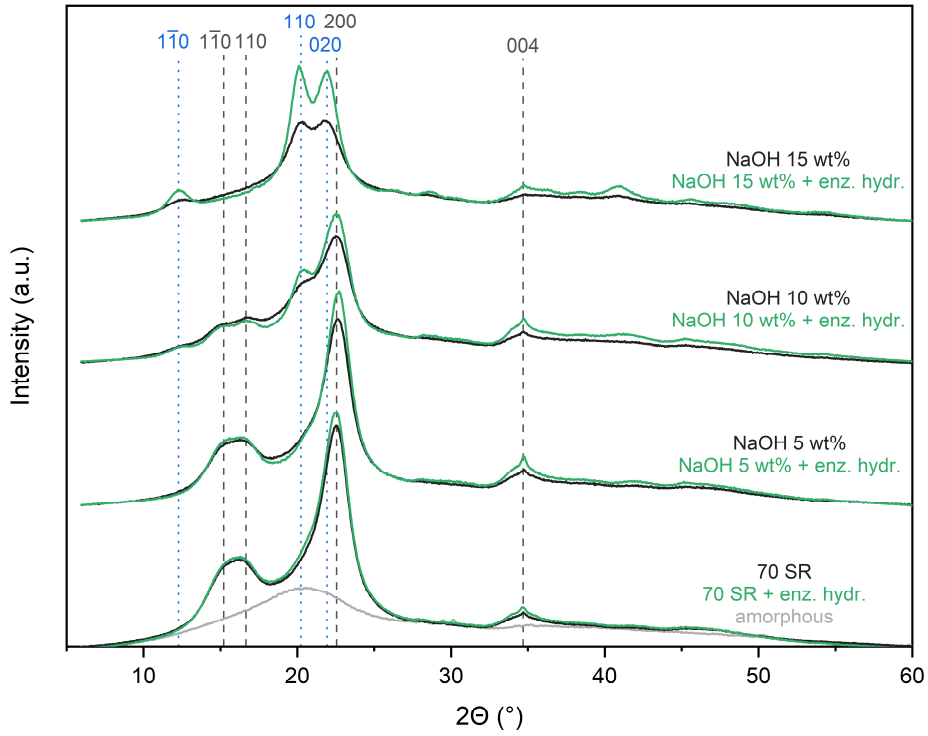

369

370 Fig. 1. X-ray diffraction patterns of eucalyptus fibers refined at 70 SR as such and after NaOH
371 treatments at several wt%, with and without additional enzymatic hydrolysis step. Characteristic
372 peaks and the associated lattice planes are indicated for Cellulose I (grey dashed lines) and Cellulose
373 II (blue dotted lines) respectively. The amorphous reference is used for the calculation of crystallinity
374 index when superimposed with the chosen pattern, as shown on the graph.

375 The following enzymatic hydrolysis step results in a global increase of the diffraction peaks intensities
376 for all samples (Fig. 1). The crystallinity indices are higher after enzymatic hydrolysis as shown in
377 Table 1, shifting from 40.7 to 45.7 % for refined fibers without NaOH treatment. This effect has been
378 widely reported and explained as a preferential action of endoglucanase on less organized cellulose
379 parts (Bansal et al., 2009; Nechyporchuk et al., 2015), although a decrease of CI due to enzymatic
380 hydrolysis is also possible (Le Moigne et al., 2010). The same trend is observed with NaOH treated
381 samples, with the most significant increase for the sample treated with NaOH 15 wt%, which has a CI
382 of 18.0 and 28.3 % before and after enzymatic hydrolysis respectively. Samples treated with NaOH 5
383 wt% and 10 wt% exhibit smaller increases of CI with the use of enzymes, from 30.2 to 34.9 % and
384 from 22.4 to 25.9 % respectively.

385 The enhancement of the efficiency of enzymatic hydrolysis for sample treated with NaOH 15 wt% is
386 due to two concurrent factors. On one hand, the hydrolysis rate tends to increase when the CI
387 decreases (SriBala et al., 2016). Enzymatic hydrolysis is thus facilitated for samples with a high

content of amorphous cellulose, due to a better accessibility of the cellulose chains. On the other hand, it has been reported that enzymatic hydrolysis is accelerated by the conversion from cellulose I to cellulose II (SriBala et al., 2016; Wada et al., 2010). The cellulose I structure consists in sheets composed of parallel cellulose chains held by hydrogen bonds. These sheets are stacked together by hydrophobic interactions such as van der Waals forces, without any intersheet hydrogen bond. The cellulose II structure, however, consists in sheets composed of antiparallel cellulose chains, resulting in a greater number of hydrogen bonds. These sheets are stacked together by weaker hydrophobic interactions, as well as intersheets hydrogen bonds (Pérez & Mazeau, 2005). The partial cleavage of these hydrogen bonds in water, as well as the weaker hydrophobic interactions could explain the faster hydrolysis rate for cellulose II compared to cellulose I. However, while the NaOH 10 wt% sample contains a larger proportion of cellulose II compared to the NaOH 5 wt% sample, the enzymatic hydrolysis step has a comparable effect on the CI of both samples (+ 3.5 and + 4.7 % respectively). For the NaOH 10 wt% sample, the enzymatic hydrolysis is also associated with a decrease of the disordered cellulose content, as shown by the decrease of the minimum at 2θ = 17.5°. This decrease influences the calculation of CI with the area-based method. The crystallinity of this sample was therefore further studied by CP-MAS nuclear magnetic resonance (NMR).

^{13}C NMR spectra were acquired for untreated 70 SR refined fibers, and fibers treated with NaOH 10 wt%, before and after enzymatic hydrolysis (Fig. 2). The spectrum of untreated 70 SR sample is characteristic of the cellulose I structure. The observed peaks can be assigned to the different carbons of the anhydroglucose unit, with the contribution of C_1 (104.7 ppm), C_2 (71.4 ppm), C_3 (74.9 ppm), C_4 (82.4 ppm for disordered cellulose, 88.9 ppm for crystalline cellulose), C_5 (72.2 ppm) and C_6 (62.5 and 64.9 ppm) (Foster et al., 2018; Kamide et al., 1984; Kono et al., 2004). The spectrum of the NaOH 10 wt% treated sample confirms the presence of cellulose II, while the remaining cellulose I peaks attest that the crystalline conversion is only partial. The intensity of cellulose I peaks decreased for the contributions of C_1, C_4 and C_6. Characteristic peaks of cellulose II can be observed at 107.2 ppm, 87.9 ppm and 62.2 ppm, associated with C_1, C_4 and C_6, respectively (Dinand et al., 2002; Hesse & Jäger, 2005). Further enzymatic hydrolysis does not lead to a change in the crystalline structure, but to a magnification of the peaks corresponding to the contribution of crystalline cellulose, at 87.9 ppm and 88.9 ppm for cellulose II and I respectively.

The clear separation of crystalline and disordered contributions for C_4 allows the calculation of a NMR crystallinity index (Table 1) with an area-based method (Foster et al., 2018; Park et al., 2010). A CI of 38 % is obtained for refined fibers, which is comparable to the value obtained with XRD (40.7 %). Here, the two techniques lead to similar values, the NMR value being slightly lower as specified in several other publications (Foster et al., 2018; Park et al., 2010). The NaOH 10 wt% treatment leads

to a decrease of the CI to 33 %. This trend is consistent with the XRD results and confirms the disruption of the cellulose structure during its crystalline conversion. The preferential action of endoglucanase on disordered cellulose is attested by the significant increase of CI after enzymatic hydrolysis, from 33 to 48 %. The CI values obtained with NMR for the NaOH 10 wt% samples, which contain both cellulose I and II, are significantly higher compared to the CI obtained with XRD. The disagreement between data deduced from NMR and those calculated from XRD could be explained by the unsuitability of NMR analysis concerning the amorphous zone of cellulose II. It was reported that the disordered C_4 of cellulose II have a lower contribution compared to cellulose I (Kono et al., 2004; Sèbe et al., 2012) which leads to overestimated crystallinity indices.

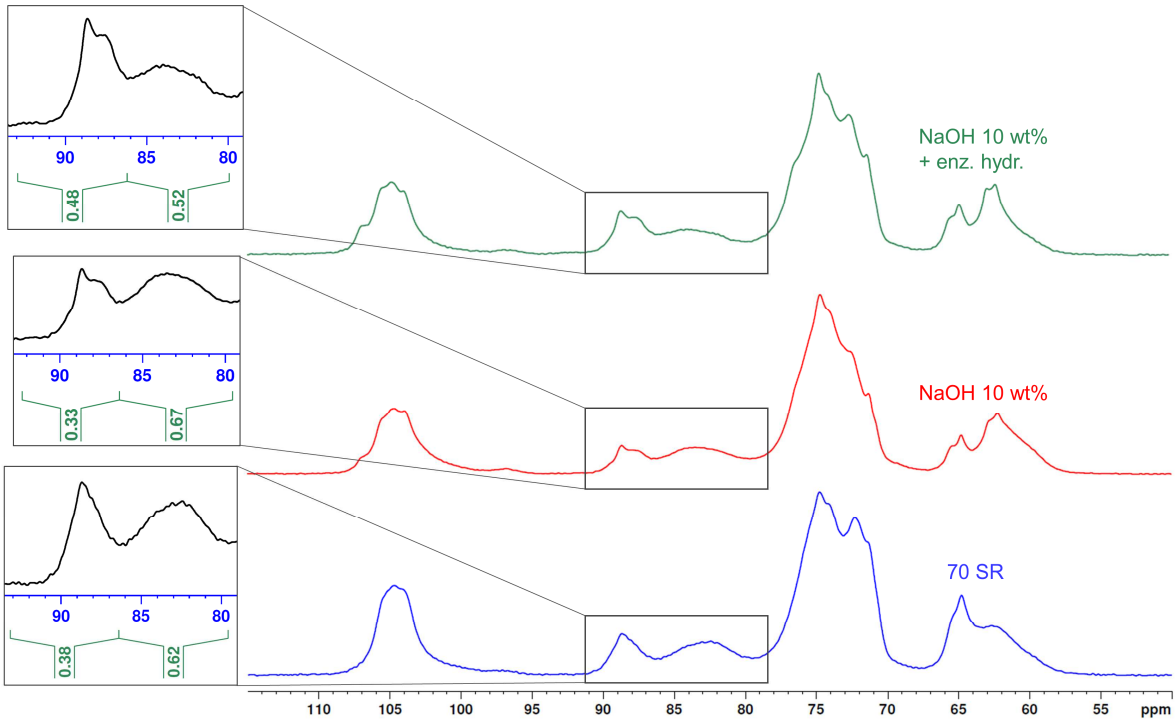

Fig. 2. Solid-state 13C CP-MAS NMR spectra of eucalyptus fibers refined at 70 SR as such, after NaOH 10 wt% treatment and after NaOH 10 wt% treatment followed by enzymatic hydrolysis. C4 crystalline (93.0 – 86.2 ppm) and disordered contributions (86.2 – 80.0 ppm) are used for the calculation of crystallinity index.

The degree of polymerization (DP) and process yield were studied for each treatment (Table 1). The enzymatic treatment alone on refined pulp leads to a major reduction of DP, from 963 to 430. A comparable decrease is observed for NaOH treatments, due to cellulose surface peeling and alkaline hydrolysis (Mozdyniewicz et al., 2013). The influence of NaOH concentration on DP is low, but is correlated to the reaction yields, the higher the concentration the lower the yield. The chemical composition of the NaOH 10 wt% treated sample underlines that the decrease of yield (85.4 %)

comes from the solubilization of a large part of hemicelluloses. The hemicellulose content shifts from 16.2 % for the untreated pulp to 1.8 % after treatment. Most of hemicelluloses are indeed soluble in NaOH-water based solvents (Budtova & Navard, 2016), and the decrease of yield with increasing NaOH concentration is linked to the increasing amount of solubilized hemicelluloses. The yield after NaOH 15 wt% treatment (78.2 %) is lower than the initial cellulose content in the pulp (83.4 %), which shows that a fraction of cellulose is removed during the treatment. This result supports the assertion of a facilitated cellulose degradation with increasing NaOH concentrations (SriBala et al., 2016). The NaOH 10 wt% treatment is also associated with a decrease in the lignin content from 0.40 to 0.27 %. The effect of following enzymatic hydrolysis is highly correlated to the NaOH concentration during alkaline treatment. After enzymatic hydrolysis, the DP shifts from 434 to 340 for NaOH 5 wt%, from 501 to 190 for NaOH 10 wt% and from 401 to 166 for NaOH 15 wt%. The efficiency of enzymes is therefore clearly improved for these samples, attesting a better cellulose accessibility due to higher disordered cellulose content and cellulose II structure. The hemicellulose content after NaOH 10 wt% and enzymatic treatment is below 1 %, and the lignin content decreases to 0.25 %. This treatment leads therefore to a purification of the pulp. Although all yield values are higher than 70 %, these values are significantly lower than for enzymatic hydrolysis of untreated sample (92.3 %). The improvement of enzymatic hydrolysis is therefore irremediably associated with a higher loss of matter during process.

Table 1

Structural properties of fibers and process yields after the different pretreatments.

	70 SR	70 SR + enz. hydr.	NaOH 5 wt%	NaOH 10 wt%	NaOH 15 wt%	NaOH 5 wt% + enz. hydr.	NaOH 10 wt% + enz. hydr.	NaOH 15 wt% + enz. hydr.
CI (%) - XRD	40.7	45.7	30.2	22.4	18.0	34.9	25.9	28.3
CI (%) - NMR	38	-	-	33	-	-	48	-
DP	963 ± 2	430 ± 1	434 ± 14	501 ± 4	401 ± 6	340 ± 2	190 ± 1	166 ± 2
Cellulose (%)	83.4	-	-	97.9	-	-	98.8	-
Hemicellulose (%)	16.2 *	-	-	1.8 *	-	-	< 1 *	-
Lignin (%)	0.40	-	-	0.27	-	-	0.25	-
Yield (%)	-	92.3	100.0	85.4	78.2	82.7	73.3	72.0

* estimated values

3.2 Morphological changes after NaOH and enzymatic treatments

The morphology of cellulose fibers after NaOH treatments was studied by scanning electron microscopy (Fig. 3). Before alkaline treatment, eucalyptus fibers have a relatively flat shape with fibrillated surfaces due to refining. A network of micrometric elements can be seen on Fig. 3a, which is characteristic of extensive refining and leads to an improvement of the fibers mechanical properties. NaOH treatments all lead to a global swelling of fibers with a relative smoothing of fiber surface (Nam & Condon, 2014). This effect was clearly visible for NaOH 10 and 15 wt% treatments (Fig. 3c and Fig. 3d respectively) with important curvature of fibers and partial destruction of the fiber structure. The irregularities of fiber surfaces seem to be due to the aggregation of micrometric elements and the apparition of kinks (Fig. 3b).

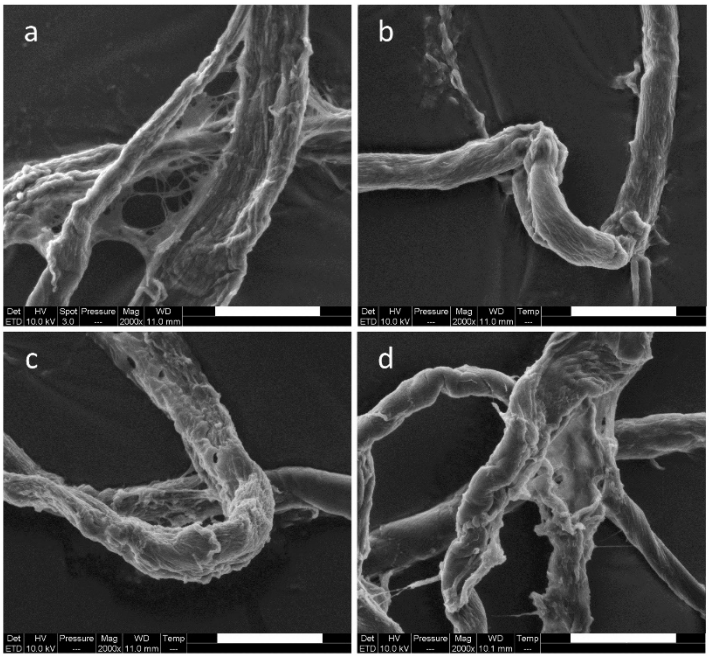

Fig. 3. SEM images of eucalyptus fibers refined at 70 SR as such (a), after NaOH 5 wt% treatment (b), after NaOH 10 wt% treatment (c) and after NaOH 15 wt% treatment (d). Scale bar is 20 µm.

The morphological changes were further studied by MorFi analysis (Fig. 4). Average fiber length and fine content (elements with length < 200 µm) were determined after each treatment, associated or not with Ultra Turrax fibrillation. This mild mechanical treatment compared to literature (Nechyporchuk et al., 2016) was chosen because of the small available quantity of cellulose fibers after each treatment (5g). It is used as a first step for fiber deconstruction towards the production of CNF, and enables to comparatively assess the efficiency of each treatment. The objective of this mild mechanical fibrillation was therefore to determine an optimum in the pretreatment conditions, to further adapt these conditions to the pilot scale grinding process.

The NaOH treatments alone have little impact on both fiber length and fine content, independently of NaOH concentration. Average fiber length shifts from 553 to 452 µm after NaOH 15 wt% treatment, although major structural changes and DP reduction have been noticed (Table 1). This attests that these structural changes have little influence on micrometric scale. Additionally, alkaline treatments do not seem to weaken the fibers enough for an efficient fibrillation, as attested by the weak impact of further Ultra Turrax treatment on fiber morphology. This low fibrillation efficiency is consistent with previous studies and could be caused by interdigitation of the cellulose nanofibrils in the cell wall (Wang et al., 2014).

The additional enzymatic hydrolysis step results in important changes in fiber morphology. Its effect on untreated pulp is already noticeable, with a reduction in fiber length to 516 µm and an increase of fine content from 15.7 to 19.0 %. This effect is enhanced on NaOH treated samples, leading to average fiber lengths of 507, 391 and 394 µm for fibers treated with NaOH 5, 10 and 15 wt% respectively. The creation of fine elements is not noticeable for NaOH 5 wt%, but is observed for NaOH 10 and 15 wt%, with fine contents of 35.6 and 38.0 % respectively. These results support the fact that the structural changes due to enzymatic hydrolysis have an impact on a micrometric scale. Here, the important DP reduction is correlated with a decrease in the fiber length, and a destructuration of the cell wall leading to fine elements. Interestingly, the subsequent Ultra Turrax step was found to be more efficient for combinations of NaOH and enzymatic treatments. After enzymatic hydrolysis and Ultra Turrax treatment, the samples treated with NaOH 5, 10 an 15 wt% exhibit fiber lengths of 466, 304 and 324 µm, and fine content of 22.0, 70.0 and 62.6 % respectively. An optimum is reached with the NaOH 10 wt% sample which has the lowest average fiber length and highest fine content. On one hand, the low fiber lengths demonstrate that these fibers are efficiently weakened and can be easily cut with a mechanical process. On the other hand, the creation of fine elements indicates the creation of cellulose microfibrils, and probable nanofibrils which cannot be detected with the apparatus. This optimum indicates the positive impact of the conversion from cellulose I to cellulose II for enzymatic hydrolysis and further deconstruction with a mechanical process, wich is more effective with NaOH 10 wt% (partial conversion) than with NaOH 5 wt% (small conversion). However, the total conversion with NaOH 15 wt% seems to lead to fiber aggregation, which has a negative impact on their deconstruction and the creation of CNF.

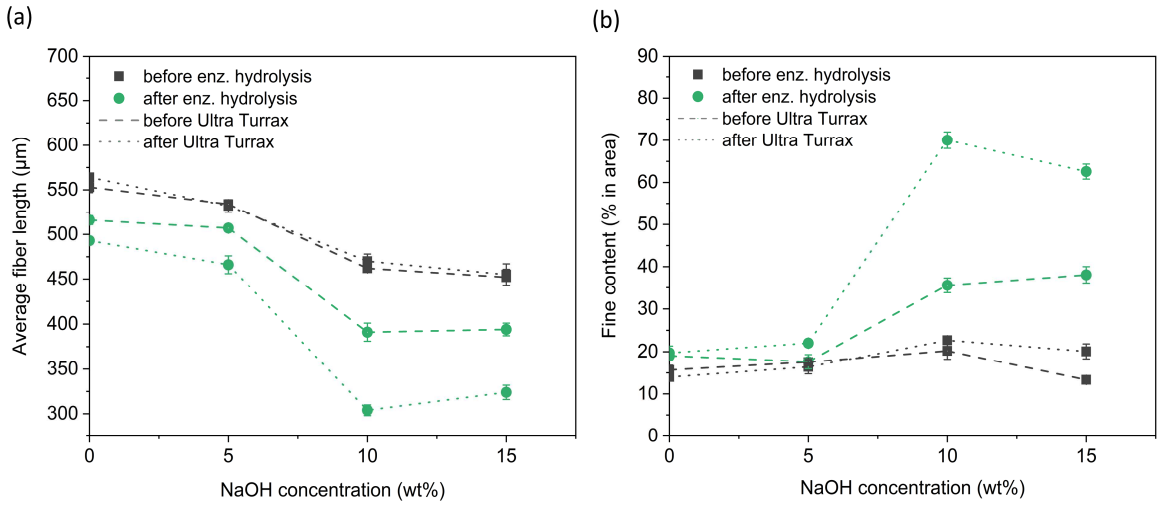

514

515 Fig. 4. Average fiber length (a) and fine content (b) obtained with MorFi analyzer, as functions of
516 NaOH concentration during treatment. The influence of enzymatic hydrolysis and Ultra Turrax steps
517 is studied, alone and in combinations. Dashed lines are guides to the eye.

518 The morphological analysis was completed by SEM images at different stages of the process (Fig. 5).
519 The impact of each step (NaOH treatment, enzymatic hydrolysis, Ultra Turrax treatment) was
520 determined, alone and in combinations. Enzymatic hydrolysis leads to fiber cutting and creation of
521 fine elements for both untreated and NaOH treated samples (Fig. 5b and Fig. 5f respectively). This
522 effect is more visible on the NaOH treated sample, as the initial fine elements from refined pulp are
523 aggregated during alkaline treatment. The effect of Ultra Turrax treatment alone (Fig. 5c and Fig. 5g)
524 is comparable for untreated and treated fibers, and leads to a destruction of the fiber structure in
525 localized positions. The fibrous structure is clearly attacked for the NaOH sample, which exhibits an
526 aggregation of cellulose fibers and microfibrils.

527 A major difference was observed in the morphology of untreated and NaOH treated fibers after
528 enzymatic hydrolysis and Ultra Turrax fibrillation. Fibers without NaOH treatment, after further
529 enzymatic and Ultra Turrax treatments, exhibit a destroyed structure and fiber aggregation, but only
530 few micrometric elements (Fig. 5d). In contrast, sample with coupled NaOH and enzymatic
531 treatment, followed by Ultra Turrax treatment, exhibits a network structure of micro- and
532 nanometric elements (Fig. 5h). The sample is relatively homogeneous, with several residual fiber
533 fragments. Remarkably, this conversion to a micro- nanometric network with the mild mechanical
534 treatment was observed for the coupled NaOH and enzymatic treatment only, and not for the NaOH
535 treatment alone (Fig. 5g) or enzymatic treatment alone (Fig. 5c). This combination seems, therefore,
536 to overcome the fibrillation issue encountered with NaOH treatments (Abe, 2016; Wang et al., 2014),
537 and to facilitate the fibrillation of enzymatically treated fibers. This encouraging result was observed

for the NaOH 10 wt% only, and was not as effective for the NaOH 5 and 15 wt% samples (results not shown here). This confirms that the partial conversion to a cellulose II structure (NaOH 10 wt%) is more efficient than a small (NaOH 5 wt%) or a total conversion (NaOH 15 wt%) for CNF production. This effect could be due to the positive impact of fiber disruption during crystalline conversion as shown with XRD and NMR, while limiting the fiber aggregation observed for high NaOH concentrations.

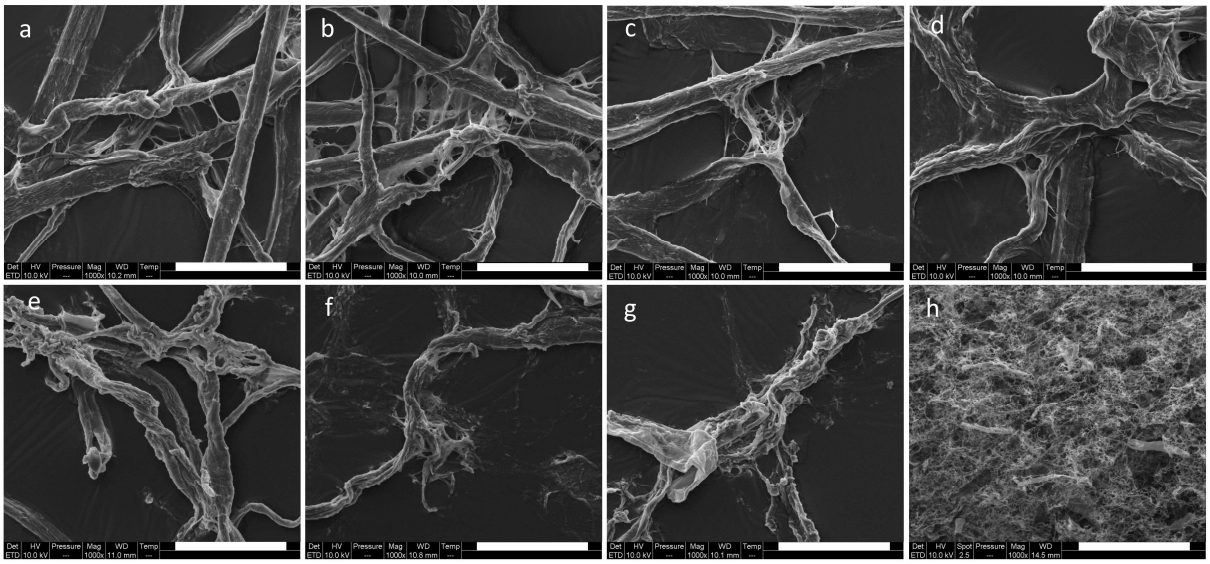

Fig. 5. SEM images of eucalyptus fibers refined at 70 SR (a – d) and after NaOH 10 wt% treatment (e – h), without further treatment (a, e), after enzymatic hydrolysis alone (b, f), after Ultra Turrax treatment alone (c, g) and after coupled enzymatic hydrolysis and Ultra Turrax treatment (d, h) respectively. Scale bar is 50 µm.

3.3 Cellulose nanofibrils properties

Based on the morphological study of fibers, NaOH 10 wt% pretreatment on one hand, and coupled NaOH 10 wt% and enzymatic pretreatment on the other hand, were used for CNF production using an ultra-fine friction grinder. The morphology of the obtained CNF was studied at different scales using optical microscopy, scanning and transmission electron microscopy (Fig. 6).

Both treatments lead to an efficient fibrillation into micro- and nano-scale elements, with few residual fragments visible by optical microscopy (Fig. 6b and Fig. 6f). SEM images reveal however major differences in the CNF structures. The NaOH treatment alone leads to an aggregation of CNF in a matrix of disordered cellulose (Fig. 6c). The analysis of TEM images (Fig. 6d) enable to determine that these CNF are composed of bundles of elementary fibrils, with widths between 30 - 100 nm and

lengths superior to 1 µm. These observations are consistent with previous findings on the difficulty to indivualize cellulose II CNF after an alkaline treatment (Abe, 2016; Wang et al., 2014). In contrast, the combined NaOH and enzymatic treatment leads to well individualized CNF, with few micrometric fiber fragments visible on SEM images (Fig. 6g). Further observations with TEM (Fig. 6h) reveal CNF composed of only few elementary fibrils, with widths between 10 - 20 nm and lengths between 150 - 350 nm, close to the dimensions of cellulose nanocrystals (Nechyporchuk et al., 2016). This low aspect ratio, associated with the low DP values (Table 1), is an indicator of the preferential action of the enzymes on the disordered cellulose structure produced during the crystalline conversion from cellulose I to cellulose II. The resulting CNF, with rigid structures, exhibit a high transmittance in the form of nanopaper (Fig. 6e).

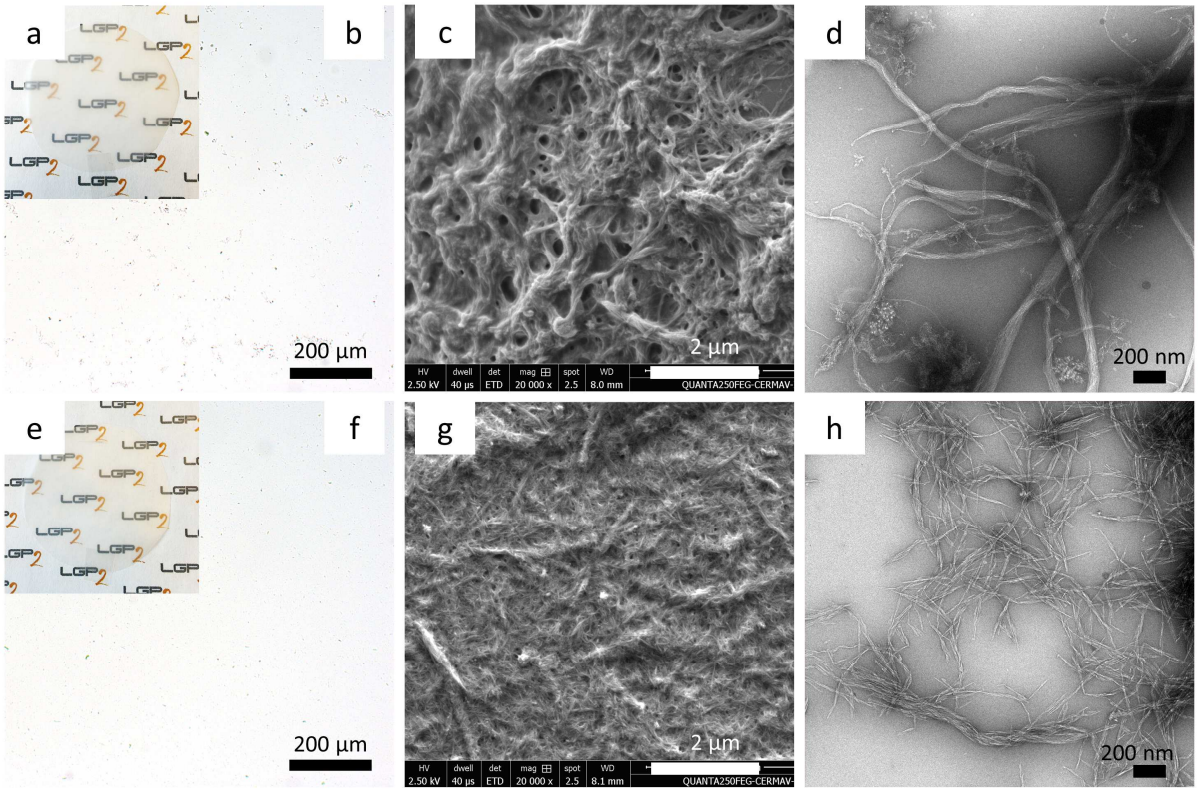

Fig. 6. Images of the resulting CNF as films and in suspension after the NaOH 10 wt% treatment followed by the grinding process (a-d) or the NaOH 10 wt% and enzymatic treatment followed by the grinding process (e-h). The associated specific energy consumptions are 23.0 and 15.5 MWh/t, respectively. Nanopapers (a, e) have a basis weight of 60 g/m², optical microscopy images (b, f) were acquired on 0.1 wt% suspensions, SEM images (c, g) were acquired on 0.1 wt% suspensions after vacuum drying and TEM images (d, h) were acquired on the supernatant of 0.1 wt% suspensions after 24h of settling.

The optical and mechanical properties of CNF were further assessed using a multi-scale quality index (Fig. 7a). The properties of CNF for each pretreatment after the highest number of passes through the grinder are detailed in Table 2. A previous study using enzymatic hydrolysis alone with similar grinding treatment was used as a reference (Desmaisons et al., 2017). For enzymatic hydrolysis alone, the quality index undergoes a fast increase with the increase of specific energy consumption, as the cellulose fibers start being deconstructed in the grinding process. As expected, this reflects a good efficiency of this pretreatment (Henriksson et al., 2007; Pääkkö et al., 2007) and an effective fragilisation of the fibers. The gradual decrease of the size of cellulose fibrous elements leads to higher energy needs for their deconstruction, resulting in a slower increase rate of the CNF properties (quality index shifting from 66.9 to 73.2 for energy consumptions of 5.1 and 11.0 MWh/t respectively). The final quality index for enzymatic treatment alone is 75.0, associated with a specific energy consumption of 13.0 MWh/t. The NaOH 10 wt% alone leads to a completely different behavior in the mechanical process. The fibrillation efficiency is drastically reduced, as attested by the slow increase of quality index with the increase of specific energy consumption. Although the suspension gradually exhibited a high viscosity typical of CNF suspensions, the associated optical and mechanical properties remain lower than the reference (Table 2). The final quality index for this treatment is 54.0, associated with a specific energy consumption of 23.0 MWh/t. Interestingly, the combined NaOH 10 wt% and enzymatic treatment leads to higher quality indices compared to reference for a same energy consumption. The starting quality index before grinding process (energy of 0.6 MWh/t due to refining) is higher (37.4 compared to 16.2 for reference). The increase rate of the CNF properties is comparable, leading to a final quality index of 82.7, associated with an energy consumption of 15.5 MWh/t. This places this sample among the high quality CNF that can be found commercially (Desmaisons et al., 2017).

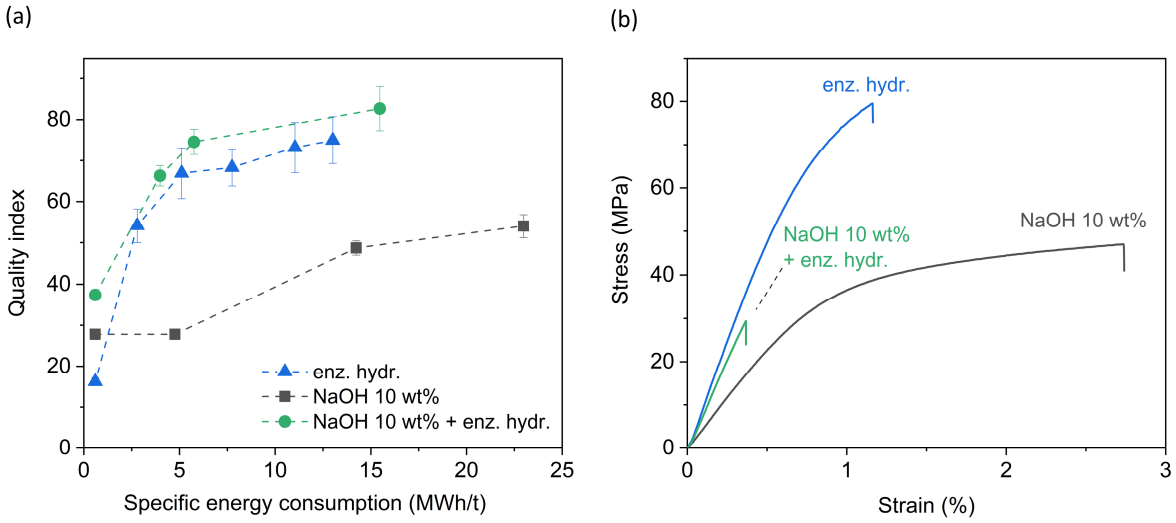

Fig. 7. Quality index as a function of specific energy consumption (a) and typical tensile curves (b) for NaOH 10 wt% treatment alone and combined NaOH 10 wt% and enzymatic treatment, compared to a reference treatment (enzymatic hydrolysis alone, values extracted from Desmaisons et al., 2017). The tensile curves refer to the CNF with the highest number of passes through the grinding process. The specific energy consumption of the refining step (0.6 MWh/t) is taken into account. Dashed lines are guides to the eye.

The tensile curves of CNF nanopapers underline the drastically different behavior of each sample (Fig. 7b). For each pretreatment, the sample with the highest energy consumption was studied, and the typical tensile curves are presented here. Enzymatic hydrolysis alone leads to nanopapers with an average tensile strength of 78 MPa, average strain at break of 1.27 %, and Young's modulus of 11.21 GPa. The Young's modulus value is in the average that can be found in the literature, as values between 8 and 15 GPa are often obtained with an enzymatic pretreatment (Benítez & Walther, 2017; Nechyporchuk et al., 2016). However, the strain and strength values are in the low average, as they are usually between 2 - 10 % and 100 - 200 MPa, respectively (Benítez & Walther, 2017). This is possibly due to the important enzyme dosage during enzymatic hydrolysis. NaOH 10 wt% treatment alone leads to a higher strain value (2.92 %), but lower stiffness (4.84 GPa) and tensile strength (50.2 MPa). The decrease of mechanical properties with the use of NaOH has been reported previously (Abe, 2019; Wang et al., 2014). This trend is due to several concomitant factors, namely (i) the removal of hemicelluloses (Table 1), which is expected to decrease the elastic modulus and tensile strength (Carvalho et al., 2019), (ii) the lower elastic modulus of cellulose II compared to cellulose I (Nishino et al., 1995), and (iii) CNF aggregation during alkaline treatment (Abe & Yano, 2011). The combined NaOH 10 wt% and enzymatic treatment results in an increase of Young's modulus (8.94 GPa) compared to NaOH alone, likely due to the partial removal of disordered cellulose during

enzymatic hydrolysis. However, both strength and strain at break are drastically reduced, with values of 30 MPa and 0.47 % respectively. This brittle behavior can be linked to the morphology of the associated CNF, which exhibit a rigid structure of relatively low aspect ratio, and do not allow any plastic deformation to occur.

Table 2

Optical and mechanical properties of cellulose nanofibrils in suspension or as nanopapers, and their associated quality index.

	Turbidity (NTU)	Transmittance (%)	Tear resistance (mN)	Young's modulus (GPa)	Porosity (%)	Quality index
Enz. hydr.	240 ± 48	7.1 ± 0.06	31 ± 9	11.21 ± 0.41	29.7 ± 2.5	75.0 ± 5.1
NaOH 10 wt%	761 ± 37	15.4 ± 1.17	27 ± 4	4.84 ± 0.20	38.5 ± 1.8	54.0 ± 2.8
NaOH 10 wt% + enz. hydr.	314 ± 13	42.2 ± 0.86	9 ± 3	8.94 ± 0.24	27.2 ± 9.5	82.7 ± 5.4

Optical and mechanical properties of CNF as suspensions or nanopapers are displayed in Table 2. The values presented here refer to the CNF with the highest number of passes through the grinding process. The associated specific energy consumptions are 13.0, 23.0 and 15.5 MWh/t for enzymatic treatment (reference, values extracted from Desmaisons et al., 2017), NaOH 10 wt% treatment and combination of NaOH 10 wt% and enzymatic treatments, respectively. The CNF aggregation caused by NaOH 10 wt% treatment alone is attested by the high turbidity (761 NTU) and porosity of the nanopaper (38.5 %). The tear resistance, however, is comparable to the reference (27 and 31 mN respectively), and the nanopapers exhibit higher transmittance (15.4 and 7.1 % respectively). The combination of NaOH 10 wt% and enzymatic treatment leads to nanopapers with similar porosity compared to reference, but lower tear resistance (9 mN) and drastically higher transmittance (42.2 %). These two properties confirm the presence of small elements with homogeneous distribution in the material. The high transmittance value could open the door to the use of this nanopaper in the packaging industry, or as a substrate for printed electronics for example, where both high transmittance and heat resistance are needed (Hoeng et al., 2016). In suspension, the turbidity is slightly higher for the combined treatment (314 NTU) compared to reference (240 NTU). The resulting CNF obtained with these various pretreatments exhibit therefore a wide range of properties, which can be favoured depending on the application.

4. Conclusions

This study confirms the positive impact of a combined NaOH and enzymatic treatment for CNF production. The structural properties of cellulose after NaOH treatments at various concentrations were assessed by XRD and ^{13}C NMR. A clear shift from a cellulose I to a cellulose II crystalline structure was observed, with a coexistence of both allomorphs for NaOH 10 wt% treated sample. The alkaline treatments were proven to improve further enzymatic hydrolysis, due to the preferential action of endoglucanase on disordered cellulose, and a faster hydrolysis rate of cellulose II compared to cellulose I as shown by DP and yield decrease. The final process yields were lower for the combined pretreatments compared to NaOH and enzymes alone, while remaining suitable for a large scale CNF production. The decrease of yields was found to be due to the solubilization of a large part of hemicelluloses during alkaline treatment, as well as a fraction of cellulose during both treatments. The morphological study by SEM and MorFi enabled to underline the positive influence of combined NaOH and enzymatic treatment on further fibrillation by a mechanical treatment. The difficulty of CNF individualization, which has been reported for CNF produced with NaOH treatment alone, was here partially overcame. An optimum was found for a NaOH concentration of 10 wt%, suggesting a positive influence of the coexistence of cellulose I and II for further enzymatic hydrolysis and fiber degradation to CNF. The production of CNF with a pilot scale grinder confirmed the positive influence of the combined treatment compared to NaOH and enzymatic treatments alone, with an increase in the quality index and a decrease of energy consumption. This combined treatment results in well individualized CNF, with rigid structures and relatively low aspect ratio. On one hand, the study of their mechanical properties underlined an important decrease of tensile strength and strain for the combined treatment under the form of nanopaper, while maintaining a stiffness comparable to the reference. On the other hand, the optical properties were found to be substantially improved. This new pretreatment could therefore be used for CNF production with tunable properties for various applications, the high transparency being an asset for their use in the packaging industry, or for high-added value applications such as substrates for printed electronics. Finally, this pretreatment could be suitable for industrial production thanks to the decrease of energy needs.

Acknowledgments

The authors gratefully thank the Association Nationale Recherche Technologie (ANRT) and Arjowiggins France SAS for financial and material support for the PhD thesis. LGP2 is part of the LabEx Tec 21 (Investissements d'Avenir - grant agreement n°ANR-11-LABX-0030) and of PolyNat Carnot Institute (Investissements d'Avenir - grant agreement n° ANR-16-CARN-0025-01). This research was made possible thanks to the facilities of the TekLiCell platform funded by the Région Rhône-Alpes (ERDF: European regional development fund). The authors thank the NanoBio-ICMG Platform (FR 2607, Grenoble) for granting access to the Electron Microscopy facility, Jean-Luc Putaux

686 and Christine Lancelon-Pin from Cermav for the TEM and SEM images, Marie-Christine Brochier-
687 Salon for the NMR spectra, Ramzi Khiari for the chemical compositions, and Thierry Encinas from
688 CMTC - Grenoble for the XRD analysis.

689 References

690 Abe, K. (2016). Nanofibrillation of dried pulp in NaOH solutions using bead milling. *Cellulose*, *23*(2),
691 1257–1261. https://doi.org/10.1007/s10570-016-0891-4

692 Abe, K. (2019). Novel fabrication of high-modulus cellulose-based films by nanofibrillation under
693 alkaline conditions. *Carbohydrate Polymers*, *205*, 488–491.
694 https://doi.org/10.1016/j.carbpol.2018.10.069

695 Abe, K., & Yano, H. (2011). Formation of hydrogels from cellulose nanofibers. *Carbohydrate Polymers*,
696 *85*(4), 733–737. https://doi.org/10.1016/j.carbpol.2011.03.028

697 Abe, K., & Yano, H. (2012). Cellulose nanofiber-based hydrogels with high mechanical strength.
698 *Cellulose*, *19*(6), 1907–1912. https://doi.org/10.1007/s10570-012-9784-3

699 Ahvenainen, P., Kontro, I., & Svedström, K. (2016). Comparison of sample crystallinity determination
700 methods by X-ray diffraction for challenging cellulose I materials. *Cellulose*, *23*(2), 1073–
701 1086. https://doi.org/10.1007/s10570-016-0881-6

702 Assis, C. A. de, Iglesias, M. C., Bilodeau, M., Johnson, D., Phillips, R., Peresin, M. S., Bilek, E. M. (Ted),
703 Rojas, O. J., Venditti, R., & Gonzalez, R. (2018). Cellulose micro- and nanofibrils (CMNF)
704 manufacturing—Financial and risk assessment. *Biofuels, Bioproducts and Biorefining*, *12*(2),
705 251–264. https://doi.org/10.1002/bbb.1835

706 Azeredo, H. M. C., Rosa, M. F., & Mattoso, L. H. C. (2017). Nanocellulose in bio-based food packaging
707 applications. *Industrial Crops and Products*, *97*, 664–671.
708 https://doi.org/10.1016/j.indcrop.2016.03.013

709 Bansal, P., Hall, M., Realff, M. J., Lee, J. H., & Bommarius, A. S. (2009). Modeling cellulase kinetics on
710 lignocellulosic substrates. *Biotechnology Advances*, *27*(6), 833–848.
711 https://doi.org/10.1016/j.biotechadv.2009.06.005

712 Benítez, A. J., & Walther, A. (2017). Cellulose nanofibril nanopapers and bioinspired nanocomposites:
713 A review to understand the mechanical property space. *Journal of Materials Chemistry A*,
714 *5*(31), 16003–16024. https://doi.org/10.1039/C7TA02006F
715 Budtova, T., & Navard, P. (2016). Cellulose in NaOH–water based solvents: A review. *Cellulose*, *23*(1),
716 5–55. https://doi.org/10.1007/s10570-015-0779-8
717 Carvalho, D. M. de, Moser, C., Lindström, M. E., & Sevastyanova, O. (2019). Impact of the chemical
718 composition of cellulosic materials on the nanofibrillation process and nanopaper properties.
719 *Industrial Crops and Products*, *127*, 203–211. https://doi.org/10.1016/j.indcrop.2018.10.052
720 Desmaisons, J., Boutonnet, E., Rueff, M., Dufresne, A., & Bras, J. (2017). A new quality index for
721 benchmarking of different cellulose nanofibrils. *Carbohydrate Polymers*, *174*, 318–329.
722 https://doi.org/10.1016/j.carbpol.2017.06.032
723 Dinand, E., Vignon, M., Chanzy, H., & Heux, L. (2002). Mercerization of primary wall cellulose and its
724 implication for the conversion of cellulose I→cellulose II. *Cellulose*, *9*(1), 7–18.
725 https://doi.org/10.1023/A:1015877021688
726 Ferrer, A., Pal, L., & Hubbe, M. (2017). Nanocellulose in packaging: Advances in barrier layer
727 technologies. *Industrial Crops and Products*, *95*, 574–582.
728 https://doi.org/10.1016/j.indcrop.2016.11.012
729 Foster, E. J., Moon, R. J., Agarwal, U. P., Bortner, M. J., Bras, J., Camarero-Espinosa, S., Chan, K. J.,
730 Clift, M. J. D., Cranston, E. D., Eichhorn, S. J., Fox, D. M., Hamad, W. Y., Heux, L., Jean, B.,
731 Korey, M., Nieh, W., Ong, K. J., Reid, M. S., Renneckar, S., … Youngblood, J. (2018). Current
732 characterization methods for cellulose nanomaterials. *Chemical Society Reviews*, *47*(8),
733 2609–2679. https://doi.org/10.1039/C6CS00895J
734 French, A. D. (2014). Idealized powder diffraction patterns for cellulose polymorphs. *Cellulose*, *21*(2),
735 885–896. https://doi.org/10.1007/s10570-013-0030-4

Gong, J., Li, J., Xu, J., Xiang, Z., & Mo, L. (2017). Research on cellulose nanocrystals produced from cellulose sources with various polymorphs. *RSC Advances*, *7*(53), 33486–33493. https://doi.org/10.1039/C7RA06222B

Henriksson, M., Henriksson, G., Berglund, L. A., & Lindström, T. (2007). An environmentally friendly method for enzyme-assisted preparation of microfibrillated cellulose (MFC) nanofibers. *European Polymer Journal*, *43*(8), 3434–3441. https://doi.org/10.1016/j.eurpolymj.2007.05.038

Hesse, S., & Jäger, C. (2005). Determination of the 13C chemical shift anisotropies of cellulose I and cellulose II. *Cellulose*, *12*(1), 5–14. https://doi.org/10.1007/s10570-004-0211-2

Hoeng, F., Denneulin, A., & Bras, J. (2016). Use of nanocellulose in printed electronics: A review. *Nanoscale*, *8*(27), 13131–13154. https://doi.org/10.1039/C6NR03054H

Hu, J., Tian, D., Renneckar, S., & Saddler, J. N. (2018). Enzyme mediated nanofibrillation of cellulose by the synergistic actions of an endoglucanase, lytic polysaccharide monooxygenase (LPMO) and xylanase. *Scientific Reports*, *8*(1), 3195. https://doi.org/10.1038/s41598-018-21016-6

Inamochi, T., Funahashi, R., Nakamura, Y., Saito, T., & Isogai, A. (2017). Effect of coexisting salt on TEMPO-mediated oxidation of wood cellulose for preparation of nanocellulose. *Cellulose*, *24*(9), 4097–4101. https://doi.org/10.1007/s10570-017-1402-y

Kaldéus, T., Larsson, P. T., Boujemaoui, A., & Malmström, E. (2018). One-pot preparation of bi-functional cellulose nanofibrils. *Cellulose*, *25*(12), 7031–7042. https://doi.org/10.1007/s10570-018-2066-y

Kamide, K., Okajima, K., Matsui, T., & Kowsaka, K. (1984). Study on the Solubility of Cellulose in Aqueous Alkali Solution by Deuteration IR and 13 C NMR. *Polymer Journal*, *16*(12), 857–866. https://doi.org/10.1295/polymj.16.857

Kobayashi, K., Kimura, S., Kim, U.-J., Tokuyasu, K., & Wada, M. (2012). Enzymatic hydrolysis of cellulose hydrates. *Cellulose*, *19*(3), 967–974. https://doi.org/10.1007/s10570-012-9696-2

761 Kono, H., Numata, Y., Erata, T., & Takai, M. (2004). 13C and 1H Resonance Assignment of Mercerized
762 Cellulose II by Two-Dimensional MAS NMR Spectroscopies. *Macromolecules*, *37*(14), 5310–
763 5316. https://doi.org/10.1021/ma030465k
764 Kuo, C.-H., & Lee, C.-K. (2009). Enhancement of enzymatic saccharification of cellulose by cellulose
765 dissolution pretreatments. *Carbohydrate Polymers*, *77*(1), 41–46.
766 https://doi.org/10.1016/j.carbpol.2008.12.003
767 Le Moigne, N., Jardeby, K., & Navard, P. (2010). Structural changes and alkaline solubility of wood
768 cellulose fibers after enzymatic peeling treatment. *Carbohydrate Polymers*, *79*(2), 325–332.
769 https://doi.org/10.1016/j.carbpol.2009.08.009
770 Lee, H., Sundaram, J., Zhu, L., Zhao, Y., & Mani, S. (2018). Improved thermal stability of cellulose
771 nanofibrils using low-concentration alkaline pretreatment. *Carbohydrate Polymers*, *181*, 506–
772 513. https://doi.org/10.1016/j.carbpol.2017.08.119
773 Ling, Z., Chen, S., Zhang, X., & Xu, F. (2017). Exploring crystalline-structural variations of cellulose
774 during alkaline pretreatment for enhanced enzymatic hydrolysis. *Bioresource Technology*,
775 *224*, 611–617. https://doi.org/10.1016/j.biortech.2016.10.064
776 Liu, Y., & Hu, H. (2008). X-ray diffraction study of bamboo fibers treated with NaOH. *Fibers and*
777 *Polymers*, *9*(6), 735–739. https://doi.org/10.1007/s12221-008-0115-0
778 Martelli-Tosi, M., Torricillas, M. da S., Martins, M. A., Assis, O. B. G. de, & Tapia-Blácido, D. R. (2016,
779 September 5). *Using Commercial Enzymes to Produce Cellulose Nanofibers from Soybean*
780 *Straw* [Research Article]. Journal of Nanomaterials.
781 https://www.hindawi.com/journals/jnm/2016/8106814/
782 Mercer, J. (1850). *Improvements in the preparation of cotton and others fabrics and other fibrous*
783 *materials* (Patent No. 13,296).
784 Miao, C., & Hamad, W. Y. (2013). Cellulose reinforced polymer composites and nanocomposites: A
785 critical review. *Cellulose*, *20*(5), 2221–2262. https://doi.org/10.1007/s10570-013-0007-3

786 Mozdyniewicz, D. J., Nieminen, K., & Sixta, H. (2013). Alkaline steeping of dissolving pulp. Part I:
787 Cellulose degradation kinetics. *Cellulose*, *20*(3), 1437–1451. https://doi.org/10.1007/s10570-
788 013-9926-2
789 Nam, S., & Condon, B. D. (2014). Internally dispersed synthesis of uniform silver nanoparticles via in
790 situ reduction of [Ag(NH3)2]+ along natural microfibrillar substructures of cotton fiber.
791 *Cellulose*, *21*(4), 2963–2972. https://doi.org/10.1007/s10570-014-0270-y
792 Nechyporchuk, O., Belgacem, M. N., & Bras, J. (2016). Production of cellulose nanofibrils: A review of
793 recent advances. *Industrial Crops and Products*, *93*(Supplement C), 2–25.
794 https://doi.org/10.1016/j.indcrop.2016.02.016
795 Nechyporchuk, O., Pignon, F., & Belgacem, M. N. (2015). Morphological properties of nanofibrillated
796 cellulose produced using wet grinding as an ultimate fibrillation process. *Journal of Materials*
797 *Science*, *50*(2), 531–541. https://doi.org/10.1007/s10853-014-8609-1
798 Nishino, T., Takano, K., & Nakamae, K. (1995). Elastic modulus of the crystalline regions of cellulose
799 polymorphs. *Journal of Polymer Science Part B: Polymer Physics*, *33*(11), 1647–1651.
800 https://doi.org/10.1002/polb.1995.090331110
801 Pääkkö, M., Ankerfors, M., Kosonen, H., Nykänen, A., Ahola, S., Österberg, M., Ruokolainen, J., Laine,
802 J., Larsson, P. T., Ikkala, O., & Lindström, T. (2007). Enzymatic Hydrolysis Combined with
803 Mechanical Shearing and High-Pressure Homogenization for Nanoscale Cellulose Fibrils and
804 Strong Gels. *Biomacromolecules*, *8*(6), 1934–1941. https://doi.org/10.1021/bm061215p
805 Park, S., Baker, J. O., Himmel, M. E., Parilla, P. A., & Johnson, D. K. (2010). Cellulose crystallinity index:
806 Measurement techniques and their impact on interpreting cellulase performance.
807 *Biotechnology for Biofuels*, *3*(1), 10. https://doi.org/10.1186/1754-6834-3-10
808 Pérez, S., & Mazeau, K. (2005). Conformations, Structures and Morphologies of Celluloses. In
809 *Polysaccharides: Structural Diversity and Functional Versatility* (Second Edition, pp. 41–68).
810 Marcel Dekker, New York.

Rol, F., Belgacem, M. N., Gandini, A., & Bras, J. (2018). Recent advances in surface-modified cellulose nanofibrils. *Progress in Polymer Science*. https://doi.org/10.1016/j.progpolymsci.2018.09.002

Rol, F., Sillard, C., Bardet, M., Yarava, J. R., Emsley, L., Gablin, C., Léonard, D., Belgacem, N., & Bras, J. (2020). Cellulose phosphorylation comparison and analysis of phosphorate position on cellulose fibers. *Carbohydrate Polymers*, *229*, 115294. https://doi.org/10.1016/j.carbpol.2019.115294

Rol, F., Vergnes, B., El Kissi, N., & Bras, J. (2020). Nanocellulose Production by Twin-Screw Extrusion: Simulation of the Screw Profile To Increase the Productivity. *ACS Sustainable Chemistry & Engineering*, *8*(1), 50–59. https://doi.org/10.1021/acssuschemeng.9b01913

Saito, T., & Isogai, A. (2006). Introduction of aldehyde groups on surfaces of native cellulose fibers by TEMPO-mediated oxidation. *Colloids and Surfaces A: Physicochemical and Engineering Aspects*, *289*(1), 219–225. https://doi.org/10.1016/j.colsurfa.2006.04.038

Sèbe, G., Ham-Pichavant, F., Ibarboure, E., Koffi, A. L. C., & Tingaut, P. (2012). Supramolecular Structure Characterization of Cellulose II Nanowhiskers Produced by Acid Hydrolysis of Cellulose I Substrates. *Biomacromolecules*, *13*(2), 570–578. https://doi.org/10.1021/bm201777j

Siqueira, G., Tapin-Lingua, S., Bras, J., da Silva Perez, D., & Dufresne, A. (2010). Morphological investigation of nanoparticles obtained from combined mechanical shearing, and enzymatic and acid hydrolysis of sisal fibers. *Cellulose*, *17*(6), 1147–1158. https://doi.org/10.1007/s10570-010-9449-z

Spieser, H., Denneulin, A., Deganello, D., Gethin, D., Koppolu, R., & Bras, J. (2020). Cellulose nanofibrils and silver nanowires active coatings for the development of antibacterial packaging surfaces. *Carbohydrate Polymers*, *240*, 116305. https://doi.org/10.1016/j.carbpol.2020.116305

SriBala, G., Chennuru, R., Mahapatra, S., & Vinu, R. (2016). Effect of alkaline ultrasonic pretreatment on crystalline morphology and enzymatic hydrolysis of cellulose. *Cellulose*, *23*(3), 1725–1740. https://doi.org/10.1007/s10570-016-0893-2

Stevanovic, T. (2016). Chemical Composition and Properties of Wood. In *Lignocellulosic Fibers and Wood Handbook* (pp. 49–106). John Wiley & Sons, Ltd. http://onlinelibrary.wiley.com/doi/abs/10.1002/9781118773727.ch3

Taheri, H., & Samyn, P. (2016). Effect of homogenization (microfluidization) process parameters in mechanical production of micro- and nanofibrillated cellulose on its rheological and morphological properties. *Cellulose*, *23*(2), 1221–1238. https://doi.org/10.1007/s10570-016-0866-5

Tsalagkas, D., Zhai, L., Kafy, A., Kim, J. W., Kim, H. C., & Kim, J. (2018). Production of Micro- and Nanofibrillated Cellulose through an Aqueous Counter Collision System Followed by Ultrasound: Effect of Mechanical Pretreatments. *Journal of Natural Fibers*, *0*(0), 1–12. https://doi.org/10.1080/15440478.2018.1558144

Turbak, A. F., Snyder, F. W., & Sandberg, K. R. (1983). Microfibrillated cellulose, a new cellulose product: Properties, uses, and commercial potential. *Journal of Applied Polymer Science. Applied Polymer Symposium.*, *37*, 815–827.

Wada, M., Ike, M., & Tokuyasu, K. (2010). Enzymatic hydrolysis of cellulose I is greatly accelerated via its conversion to the cellulose II hydrate form. *Polymer Degradation and Stability*, *95*(4), 543–548. https://doi.org/10.1016/j.polymdegradstab.2009.12.014

Wang, H., Li, D., Yano, H., & Abe, K. (2014). Preparation of tough cellulose II nanofibers with high thermal stability from wood. *Cellulose*, *21*(3), 1505–1515. https://doi.org/10.1007/s10570-014-0222-6

Yamane, C., Abe, K., Satho, M., & Miyamoto, H. (2015). Dissolution of cellulose nanofibers in aqueous sodium hydroxide solution. *Nordic Pulp & Paper Research Journal*, *30*(1), 92–98. https://doi.org/10.3183/npprj-2015-30-01-p092-098